Optical Absorption of Small Palladium-Doped Gold Clusters

Kaydashev, Vladimir; Ferrari, Piero; Heard, Christopher; Janssens, Ewald; Johnston, Roy L.; Lievens, Peter

DOI:
10.1002/ppsc.201600036

Particle and Particle Systems Characterization

Optical absorption of small palladium doped gold clusters

--Manuscript Draft--

Manuscript Number:	ppsc.201600036R1
Full Title:	Optical absorption of small palladium doped gold clusters
Article Type:	Full Paper
Section/Category:	Advanced Particle Characterization Techniques - invitation only
Keywords:	gold clusters; palladium doping; optical absorption
Corresponding Author:	Peter Lievens, Ph.D. KU Leuven Leuven, BELGIUM
Corresponding Author Secondary Information:	
Corresponding Author's Institution:	KU Leuven
Corresponding Author's Secondary Institution:	
First Author:	Vladimir Kaydashev, Ph.D.
First Author Secondary Information:	
Order of Authors:	Vladimir Kaydashev, Ph.D.
	Piero Ferrari
	Christopher Heard
	Ewald Janssens, Ph.D.
	Roy L. Johnston
	Peter Lievens, Ph.D.
Order of Authors Secondary Information:	
Abstract:	The effect of Pd doping on the structure and optical absorption of small cationic gold clusters is investigated by a combined photodissociation spectroscopy and time-dependent density functional theory study of Aun+Arp and PdAun-1+Arp (n=4,5 ; p=0,1). While pure Au clusters are planar, the Pd doped clusters are three dimensional. UV-visible absorption is studied in the 2.0-4.7 eV photon energy range, allowing the observation of previously unreported absorption bands for Au4+ and Au4+Ar. The oscillator strength of the optical transitions is dramatically reduced upon incorporating a Pd atom in Au4+ and Au4+Ar, while this effect is less pronounced for Au5+Ar. Analysis of the electron density transfer shows a different influence of Pd with size. While Pd has a formal negative charge in Au3Pd+, in Au4Pd+ most of the charge is attracted by the highly coordinated central Au atom, leaving Pd positively charged, also affecting the induced structural changes. In addition, orbital analysis of the optical transitions was carried out in order to identify the levels involved in the optical absorption of the pure Au and Pd doped clusters. A reduction of the s density near the Fermi energy, induced by Pd doping, causes a quenching of optical absorption.
Additional Information:	
Question	**Response**
Please submit a plain text version of your cover letter here. Please note, if you are submitting a revision of your manuscript, there is an opportunity for you to provide your responses to the reviewers later; please	Dear editors Herewith we submit our manuscript entitled: “Optical absorption of small palladium doped gold clusters” as a paper for the special issue on “Advanced Particle Characterization Techniques”, upon invitation by prof. Sara Bals and prof. Luis M. Liz-Marzán.

do not add them to the cover letter.	The paper deals with a combined experimental and theoretical study of the optical properties of small gold clusters and how these properties are influenced by chemical and structural changes upon doping with a single Pd atom. The experimental work essentially is based on mass spectrometry and action spectroscopy, and the theoretical work uses density functional theory. Our findings clearly demonstrate the importance of structural changes on the electronic structure, and hence the optical properties, in such small particles. The detailed investigation reveals that charge distribution, different for different investigated sizes and compositions, plays an important role. Another observation is the strong quenching of optical absorption upon doping gold clusters with palladium. While this was investigated experimentally before, this study combined with theory revealed that this is related to the altered electronic states, in particular the significant reduction of s-d mixing when a palladium atom is incorporated. We do hope that this study on very small clusters provides an interesting and broadening contribution to the special issue of Particle, in the limit of very small particles. On behalf of the co-authors, Peter Lievens

Submitted to Particle & Particle Systems Characterization

DOI: 10.1002/ppsc.((please add manuscript number))
Article type: Full paper

Optical absorption of small palladium doped gold clusters

Vladimir Kaydashev, Piero Ferrari, Christopher Heard, Ewald Janssens, Roy L. Johnston, and Peter Lievens*

Dr. V. Kaydashev, P. Ferrari, Prof. Dr. E. Janssens, Prof. Dr. P. Lievens
Laboratory of Solid State Physics and Magnetism, KU Leuven, 3001 Leuven, Belgium
E-mail: ewald.janssens@fys.kuleuven.be
Dr. C. Heard
Department of Applied Physics, Chalmers University of Technology, Gothenburg, Sweden
Prof. Dr. R. L. Johnston
School of Chemistry, University of Birmingham, Edgbaston, Birmingham B15 2TT, UK

Keywords: gold clusters, palladium doping, optical absorption

The effect of Pd doping on the structure and optical absorption of small cationic gold clusters is investigated by a combined photodissociation spectroscopy and time-dependent density functional theory study of $Au_n^+Ar_p$ and $PdAu_{n-1}^+Ar_p$ (n=4,5 ; p=0,1). While pure Au clusters are planar, the Pd doped clusters are three dimensional. UV-visible absorption is studied in the 2.0–4.7 eV photon energy range, allowing the observation of previously unreported absorption bands for Au_4^+ and Au_4^+Ar. The oscillator strength of the optical transitions is dramatically reduced upon incorporating a Pd atom in Au_4^+ and Au_4^+Ar, while this effect is less pronounced for Au_5^+Ar. Analysis of the electron density transfer shows a different influence of Pd with size. While Pd has a formal negative charge in Au_3Pd^+, in Au_4Pd^+ most of the charge is attracted by the highly coordinated central Au atom, leaving Pd positively charged, also affecting the induced structural changes. In addition, orbital analysis of the optical transitions was carried out in order to identify the levels involved in the optical absorption of the pure Au and Pd doped clusters. A reduction of the s density near the Fermi energy, induced by Pd doping, causes a quenching of optical absorption.

1. Introduction

The unique characteristics of gold clusters and nanoparticles have received significant attention in recent decades. In particular, their optical properties and chemical reactivities are used in the design of novel environmental applications, including photo-catalytic water splitting,[1] CO oxidation,[2] molecular hydrogen dissociation[3] and the design of efficient solar cells.[4] To enhance understanding, small unsupported atomic clusters, consisting of only a few atoms, represent ideal model systems for detailed investigations.[5] Moreover, many properties of small atomic clusters do not scale with size, are strongly composition and charge dependent, and can be very different from those of bulk materials.[6] Research on clusters in the gas phase can be performed under controlled conditions and without interactions with the environment, thus providing fundamental knowledge of relevance for the understanding of more complex systems.[7]

Structural and ground state electronic properties of small Au clusters in different charge states have been largely characterized.[8-12] In addition, significant efforts have been made concerning the investigation of optical properties of clusters. Studies on mass selected clusters, e.g. Cu_n, Ag_n and Au_n have been performed in rare gas (RG) matrices, [13-16] because direct optical measurements are challenging and require advanced techniques.[17] This is a consequence of the very low density of clusters in molecular beams. Although experiments on embedded clusters in RG matrices have been successful, a drawback of this approach is that weak interactions with the rare gas matrix must be considered. An alternative is presented by photodissociation spectroscopy.[18] In this technique, laser light absorption is monitored mass spectrometrically via photon induced fragmentation, rather than by changes in light intensity. Using this method, UV-visible optical absorption was studied for several mass selected Au, Ag, and Cu clusters: $Au_4^+Ar_p$ (p = 0–4),[19] $Au_n^+Ar_p$ (n = 7; p = 0–3 and n = 8, 9; p = 0, 1),[20] Au_n^-Xe (n = 7–11),[21] Ag_4^+ and Au_4^+,[22] Ag_n^+ (n = 6, 8),[23] and Cu_3.[24] An important observation from these experiments is the rather complicated absorption features of Au clusters in contrast with Cu and Ag coinage metal clusters.[22] The heavy Au atoms are subject to significant relativistic effects resulting in a reduced valence s-d energy separation partially involving d-electrons in the absorption process.[25] Close-lying d electrons screen s electrons and thereby reduce the optical absorption bands. In contrast, the larger s-d separation in Ag allows the use of free electron models to describe its optical response, such as the plasmonic-like absorption spectra of very small Ag_n^+ (n = 4, 6, 8) clusters.[22, 23]

The properties of coinage metal clusters can be tuned by dopant atoms.[26] It has been shown that the addition of a single dopant atom can drastically change the stability,[27] reactivity,[28] and electronic properties of clusters.[29] In addition it is expected that the optical absorption of coinage metal clusters should also be drastically affected by the inclusion of dopant atoms. However, so far only a few experimental studies have dealt with this problem. In the 1990s, Morse and co-workers studied AgAu and CuAu dimers.[30,31] More recently, optical absorption measurements were carried out for $Au_{4-m}Cu_m^+$ (m = 0–2)[32] and $Ag_nAu_{4-n}^+$ (n = 1–3) clusters in the gas phase.[33]

Of particular interest are Pd doped Au clusters. Bonding between Au and Pd atoms involves promotion of at least one Pd 4d electron to a 5s orbital and thus, significant charge redistribution takes place.[34] These modifications of the electronic structure can, for instance, enhance the chemical reactivity of Au towards CO and O_2 in Au_nPd ($n \leq 7$) or lead to Pd dopant induced 2D to 3D structural transitions due to the orbital orientations provided by Pd.[35,36] Using DFT calculations, low energy structures of Pd doped gold clusters of different sizes and charge states have been predicted: Au_nPd^m (n = 1–4, m = –1,0,1),[36] Au_nPd_m ($n+m \leq 14$),[37] Au_nM (n = 1–7, M = Ni, Pd, Pt),[29] Au_nPd (n = 1–4),[38] and $Au_{32-m}Pd_m$ (m = 1, 2, 4, 6).[39]

It has been shown that also the properties of larger Au nanoparticles (2-5 nm) can be significantly modified by introduction of other metals. In particular, in the Au-Pd alloy nanoparticles an increased d-electron density at the Au sites was observed by XANES experiments, giving rise to a Au "white" line intensity decrease and decreasing Au 4f binding energies in XPS studies, evidencing the charge transfer from Pd to Au 5d orbitals.[40,41] The effect is higher when the number of Au-Pd bond increases.

Recently, some of us experimentally investigated the effect of Pd on the optical absorption of Au_n^+ ($13 \leq n \leq 20$) clusters.[42] A strong quenching effect of the absorption bands upon Pd doping was observed for all studied sizes, though with a noticeable size dependent alteration, and was attributed to dopant induced charge redistribution. In order to determine whether these effects extend down to the smallest clusters, in the current work, we investigate the effect of Pd on the optical absorption properties of Au_4^+, Au_4^+Ar and Au_5^+Ar clusters in a broad photon energy range of 2.0–4.7 eV, using a combined photodissociation spectroscopy and time-dependent density functional theory (TDDFT) approach. The calculations provide understanding of the effect of the Pd dopant on optical properties and the interplay between electronic structure and optical absorption.

2. Methods

2.1. Experimental setup and data analysis

Cationic pure gold and Pd-doped gold clusters are simultaneously produced in a dual-target dual-laser vaporization source.[43] The second harmonic of two independent Nd:YAG pulsed lasers (532 nm, 10 Hz) is used to ablate separately Au and Pd targets. Just before ablation, a small amount of He gas is introduced at 8 bar by a supersonic valve, thermalizing the ablated plasma via heat exchange between the carrier gas and the source walls, which are cooled by a constant flow of liquid nitrogen. Using a temperature controller, the source can be stabilized to any temperature in the range of 80–300 K. In this study a source temperature of 250 K is selected. A small concentration of Ar (2%) is added to the carrier gas to form cluster–Ar complexes.[44] After expansion into vacuum through a conical nozzle, the central part of the beam is selected by a skimmer and clusters enter the extraction region of a reflectron time-of-flight (TOF) mass spectrometer. Total fraction of Ar complexes for Au_n^+ and $PdAu_{n-1}^+$ (n=1-13) clusters observed in mass spectra is available in **Figure S1** of the Supporting Information.

To measure photodissociation spectra of bare clusters and their Ar complexes, the particles are excited in the extraction zone of the TOF by laser light. Tunable lasers were employed to cover the entire 2.0 to 4.7 eV photon energy range. For the 262–340 nm and 370–620 nm ranges a Nd:YAG pumped optical parametric oscillator (Quanta-Ray, MOPO-710, 10 Hz) with a BBO-crystal based frequency doubling unit (Quanta-Ray FDO-1) was used, while the 340–370 nm range was covered by a Nd:YAG pumped dye laser (Sirah Cobra Strech, 10 Hz) using Pyridine 1, Pyridine 2 and Styryl 8 as dyes and a KDP crystal for second harmonic generation. The energy per pulse is monitored by a pyroelectric energy sensor (ThorLabs, ES111C) and maintained below 5 mJ/cm^2 per pulse to avoid two-photon processes. Using a chopper, operated at 5 Hz and synchronized with the tunable lasers, mass spectra with and without laser excitation are recorded simultaneously. Each mass spectrum is an average of over 5000 cluster production cycles.

Photodepletion is measured as a function of photon energy and is defined as the ratio of the intensities of a certain species in the mass spectra recorded with (I) and without (I_0) laser excitation. Then, this ratio is converted into absorption cross section using the modified Lambert-Beer-Law:[19]

$$I/I_0 = 1 - b + b\, exp(-\sigma\Phi), \quad (1)$$

where Φ is the photon fluence, σ the absorption cross section and b a factor taking into account an imperfect spatial and temporal overlap between dissociation laser and extracted clusters. It is worth stressing that Equation 1 assumes only one-photon processes are responsible for absorption.[21] From fluence dependence curves an overlap factor *b* of 0.5 is estimated (**Figure S2** of Supporting Information).

2.2. Computational details

The density functional theory genetic algorithm (GA-DFT) global optimization approach is utilized to locate the global minimum structures of the metallic clusters, along with several energetically low-lying local minima. This approach involves the coupling of the unbiased structure prediction code, the Birmingham Cluster Genetic Algorithm (BCGA), to the plane-wave DFT electronic structure calculation package Quantum Espresso (QE).[45,46] DFT screening of cluster structures is performed with the PBE exchange-correlation functional, within the spin-unrestricted, generalized gradient DFT framework.[47] For Au and Pd atoms, 11 and 10 electrons are explicitly included in the valence, respectively, with the effect of all remaining electrons represented by ultrasoft RRKJ pseudopotentials.[48] Individual cluster convergence is achieved according to a force cutoff of 10^{-2} eV/Å and electronic self-consistency of 10^{-5} eV. Upon convergence of the BCGA, the final generation of structural candidates are subjected to geometry reoptimization within the NWCHEM v6.1 package.[49] This orbital-based method is applied with an extensive 19-electron def2-TZVPP basis set for all atoms and the corresponding effective core potential (def2-ECP) of Weigend and Ahlrichs is additionally employed for Au and Pd atoms.[50] The range-separated exchange-correlation functional LC-ωPBEh is used,[51,52] due to its recently proven good performance for the structures and optical spectra of Au and AuAg clusters in this size range.[22,33] After local reoptimization, a frequency analysis is performed for all putative global minima to verify that each is a true minimum structure. Argon tagging is performed for each global minimum metallic cluster structure, considering all symmetry-inequivalent sites and subsequently optimizing local geometry.

For minimum-energy structures resulting from the DFT optimizations, electronic excitation spectra are calculated using spin-unrestricted TDDFT considering 60 excited states. All excited state calculations are performed with NWChem, using the same exchange-correlation functional and basis set as in the geometry optimization step.[50] The output from optical response calculations is analyzed using Chemissian, an analytical tool for electronic structure and spectra calculations.[53]

3. Results

3.1. Fragmentation channels and dissociation energies

Examples of typical mass spectra with (black) and without (red) laser excitation are presented in **Figure 1**. As seen from Figure 1a and 1b, Au_4^+ and Au_4^+Ar shows signal depletion under laser excitation at wavelengths of 482 and 460 nm, respectively. The situation, however, is different for Au_3^+ (Figure 1a and 1b), showing a considerable signal increase. Several most probable fragmentation channels were assumed analysing the behaviour of mass spectra. In order to understand the clusters fragmentation behaviour under photoabsorption the lowest energy fragmentation channels of $Au_n^+Ar_m$ (n = 4, 5; m = 0, 1) and $PdAu_{n-1}^+Ar_m$ (n = 4, 5; m = 0, 1) clusters were calculated by DFT simulations and analysed together with observations. A list of channels and dissociation energies is presented in **Table 1.**

Fragmentation of Au_4^+ occurs by monomer evaporation. The calculated dissociation energy for this channel (1.33 eV) is well below the single photon energy of the experimentally investigated spectral range (2.0–4.7 eV). This result is supported by the measurements presented in Figure 1a and 1b, in which Au_4^+ depletion coincides with Au_3^+ signal increase, as also seen in previous experiments.[19,22,32] $PdAu_3^+$ preferentially dissociates by loss of a neutral Au atom, but the calculated dissociation energy (2.25 eV) is much larger and is higher than the lowest photon energy used. This should be considered when interpreting the optical absorption spectra, since bands are only observed in action spectroscopy if the single photon absorptions finally results in cluster fragmentation. For photon energies that are only slightly higher than the energy needed for dissociation, the cluster fragmentation may occur at time scales longer than those of the experiment.[54] The investigation of cluster–Ar complexes is relevant in this context since the cluster–Ar bond is weak and will break rapidly following adsorption of a single UV or visible photon. This is confirmed by the calculated Ar evaporation energies that are of the order of 0.2 eV only (Table 1), in agreement with previous calculations.[55] Actually the experiments show that the absorption of a photon by the Au_4^+Ar cluster leads to simultaneous evaporation of an Ar and a Au atom, as shown in Figure 1b. This is consistent with the low calculated energy required for this process (1.54 eV).

In contrast to Au_4^+, the lowest energy fragmentation channel of Au_5^+ is found to be dimer evaporation, with a dissociation energy of 2.17 eV. Monomer evaporation from this cluster leads to a dissociation energy of 2.74 eV, much larger than for dimer evaporation. The case of $PdAu_4^+$, however, is different. The dissociation energy of monomer evaporation is found lower, being 1.64 eV, while for dimer evaporation the larger value of 2.07 eV is obtained.

Finally, it is worth to mention that for the applied experimental conditions multiple Ar complexes are formed for Au_5^+: $Au_5^+Ar_m$ with m = 1–3, as shown in **Figure S3** of the Supporting Information. The depletion spectrum of Au_5^+Ar may be contaminated by fragmentation of $Au_5^+Ar_2$ and $Au_5^+Ar_3$, although the data suggest that all Ar atoms are evaporated simultaneously following photon adsorption and such contamination is therefore likely to be limited.

3.2. Optical absorption of Au_4^+ and $PdAu_3^+$ clusters

The calculated absorption spectra of Au_4^+ and $PdAu_3^+$ are compared with the experimental photodissociation spectra in **Figure 2**. Photon absorption cross sections are calculated as a function of excitation energy from the measured photodepletions using Equation 1. The photodepletion curves only show signal decrease, implying that the measured spectra for Au_4^+

and $PdAu_3^+$ are not contaminated by fragmentation of larger clusters. Indeed, calculated fragmentation pathways (Table 1) indicate that Au_4^+ is neither the preferred fragment of Au_5^+ nor of Au_4^+Ar, since Au_5^+ favors dimer evaporation and Au_4^+Ar evaporates simultaneously Ar and Au after photoexcitation in the measured spectral range. On the other hand, photodissociation of $PdAu_4^+$ may produce $PdAu_3^+$, but this process seems not to be likely, since no contamination observed in the spectra of $PdAu_3^+$. Due to the noise level of the measurements, features with cross sections below 0.25 Å^2 are not labeled as bands. As a standard procedure, data were averaged by 3-adjacent points in order to identify absorption features and then, based on this average, a multi-Gaussian fit was applied to the raw data. Using this criterion, four resonant excitations are observed for Au_4^+, with maxima at 2.58 eV (A), 3.49 eV (B), 3.87 eV (C) and 4.43 eV (D). Of these four bands, feature B at 3.49 eV is clearly the most intense. Previous gas phase studies of Au_4^+ were performed with photon energies below 3.5 eV and hence only reported band A at 2.58 eV,[19,20,22,32] and an onset of band B.[22] UV-visible absorption measurements of neutral mass selected gold clusters embedded in Ne matrices were carried out in the extended energy range of 1.5-6.0 eV, showing a strong absorption feature at 3.17 eV, close to band B.[16]

In order to isolate the electronic properties of the optical spectra, TDDFT calculations were performed on the energetically lowest-lying isomers as calculated with DFT. Figure 2b shows that the computed spectrum, calculated with the rhombic minimum energy structure of Au_4^+ shown as inset, is in good agreement with the experiment if a redshift of the computed bands B, C, and D of about 0.2 eV is taken into account.[19,22,32] In Ref. [22], the simulated peak at 3.3 eV was assigned to a low intensity band at 3.2 eV, and the existence of an experimental band at 3.5 eV was interpreted as the presence of additional isomers in the beam. In the current work, we suggest that the calculated peak B may be a redshifted representation of the experimental peak B. For all peaks above 3.0 eV, both in the current work and in Ref. [22], the transitions are of the same type, primarily Au 5d to Au 6s interband transitions. The computed band E at 4.42 eV is not observed experimentally. However, considering the observed redshift of the calculated bands, feature E may be present at higher energies than those measured.

The effect of substitution of Pd for Au in Au_4^+ is significant. Structurally, the Pd dopant induces a 2D → 3D transition similar to earlier calculations.[34] As commented in the introduction, the structural change is likely affected by the charge transfer expected upon Pd doping. More surprising is the completely altered optical response. Using the earlier presented criterion to identify signals with cross sections above 0.25 Å^2 as bands, only at the highest photon energies (>4.6 eV) is the onset of a band found in the experimental spectrum of $PdAu_3^+$ (Figure 2c). The calculated spectrum, shown in Figure 2d, agrees well with the experiment. Optical absorption bands are strongly suppressed, showing only an intense feature at 4.56 eV, probably corresponding to feature A observed experimentally (again considering a redshift of the computed spectrum relative to the experiment). Computations also predict a signal at 2.3 eV, which may be sufficiently intense to be measurable. However, the large dissociation energy calculated for $PdAu_3^+$ (2.25 eV) likely suppresses fragmentation following photoabsorption at low excitation energies, explaining the absence of that band in Figure 2c.

Oscillator strengths, extracted from the measured absorption cross sections, are listed in **Table 2** and compared with the calculated results.

3.3. Optical absorption of Au_4^+Ar and Au_3Pd^+Ar clusters

Figure 3 presents the experimental photodissociation and calculated optical excitation spectra of Au_4^+Ar and $PdAu_3^+Ar$. In view of the dissociation energies listed in Table 1, it seems that complexes with multiple Ar atoms loose the messenger atoms simultaneously upon photoexcitation. So possible contamination of the spectra of Au_4^+Ar and $PdAu_3^+Ar$ by dissociation of complexes with multiple Ar atoms is unlikely. Indeed, the photodissociation spectra show only signal decrease, which supports this assumption. Five bands, at energies 2.71 eV, 3.15 eV, 3.48 eV, 3.67 eV and 3.87 eV, can be distinguished in the experimental spectrum of Au_4^+Ar (Figure 3a). However, the rather high level of noise makes a clear distinction difficult. Comparing bands A of Au_4^+ (Figure 2a) and Au_4^+Ar, a blue shift of 0.1 eV is observed, as reported in previous studies.[19, 32] Band B at 3.15 eV has also been observed previously.[19] All bands above 3.4 eV are reported for the first time. The agreement with the calculated spectrum (Figure 3b) is fairly good, with minor energy shifts. The experimentally assigned bands D and E are not reproduced theoretically, which may be caused by not completely reliable band assignment in the experiment due to the low signal-to-noise level. However, another possibility is the coexistence of low-energy isomers in the beam. For this purpose the optical absorption spectrum of a y-shaped isomer was calculated and shown in blue dashed line in Figure 3b. This isomer, when Ar tagged, only is only 0.11 eV higher in energy than the global minimum and thus, could be present in the experiment. The y-shaped isomer has electronic excited states at 3.78 eV and 3.95 eV, close to the missing peaks in the experimental spectrum. All peaks for the calculated spectrum in this energy range are predominantly Au 5d – Au 6s or Au sd – Au 6s hybrid transitions.

As for the bare Au_4^+ and Au_3Pd^+ clusters, Pd doping quenches the optical absorption of the Ar complexes. Although the level of noise in the photodissociation spectrum of $PdAu_3^+Ar$ hampers definitive band assignment, features A and B of Au_4^+Ar are clearly suppressed. This observation agrees well with the calculated absorption spectrum of $PdAu_3^+Ar$, with only two weak absorption bands at 3.70 eV and 4.44 eV.

3.4. Optical absorption of Au_5^+Ar and Au_4Pd^+Ar clusters

In contrast to the photoexcitation of Au_4^+, the Au_5^+ signal in the mass spectrum shows no depletion, but only signal increase, implying that its depletion spectrum is contaminated by larger clusters dissociating into Au_5^+. Therefore, only Ar complexes of Au_5^+ and Au_4Pd^+ are discussed here. For these species the cluster-Ar_m complex peaks are depleted while the intensity of the corresponding cluster without Ar increases. As Ar atoms are weakly bound by Van der Waals forces with energy of ~0.2 eV (see Table 1) these typical action spectroscopy channels are indeed very probable.

Figure 4 displays experimental photodissociation and calculated absorption spectra for Au_5^+Ar and $PdAu_4^+Ar$. Again the Pd dopant induces a 2D to 3D structural transition, but for this cluster size the influence of the Pd dopant on the optical absorption spectrum is less pronounced. Both Au_5^+Ar (Figure 4a) and $PdAu_4^+Ar$ (Figure 4c) have an absorption feature at around 3.5 eV (band A) and no appreciable quenching upon Pd-doping is observed for this band. In addition, broad absorption features are observed for Au_5^+Ar above 4.0 eV, which are somewhat reduced in intensity by Pd doping. Calculated absorption spectra, presented in Figure 4b and 4d, show less agreement with the experiment. Calculated optical absorption of multiple Ar complexes $Au_5^+Ar_p$ (p=1-3) are available in Figure S5b of the Supporting Information. Band A is reproduced in both clusters and it is blue shifted by about 0.4 eV for Au_5^+Ar. For this cluster, two bands at 4.1 eV and 4.3 eV may represent the broad increase observed experimentally in that range, in addition to a very intense band, at 4.5 eV, calculated but not observed in the experiment. Nonetheless, this intense feature may occur at photon energies above the investigated range. Calculated features between 3.8 eV and 4.4 eV for $PdAu_4^+Ar$ cannot be distinguished from the noise level experimentally.

Although the agreement between experiment and theory is better for the tetramers than the pentamers, the different influence of Pd-doping on the optical spectra for the tetramers and pentamers is in line with the induced structural changes.

4. Discussion

4.1. Structures and charge transfers

As shown in Figure 2, 3 and 4, the structures of the Au_n^+ (n = 4, 5) clusters are affected by Pd-doping. It is known that cationic Au clusters remain planar up to n = 7 while cationic pure Pd clusters form 3D structures from n = 4 onwards.[8,56] The relativistically enhanced s-d hybridisation in gold causes an unusually large cluster size for the 2D-3D transition, as the preferential overlap of valence orbitals which minimises electronic energy is in an in-plane direction. This stabilisation is not present in palladium, and leads to compact, pseudospherical structures.[54] Thus, doping palladium atoms into gold clusters disrupts this planarity stabilisation, and drives a transformation of dimensionality from 2D to 3D. We observe, in agreement with previous studies, that this transition occurs as the smallest possible cluster size of Au_nPd_m (n+m=4). [29,58,59]

This 2D to 3D geometry change possibly diminishes the absorption cross section and is therefore partially responsible for the overall absorption quenching accompanying Pd-doping. A similar theoretical prediction of a decrease in cluster polarizability with changing Ag_n structure from planar to three-dimensional at n = 7 has been discussed previously.[60]

To analyse the charge transfer in more detail, electron densities are calculated. The results according to the Löwdin scheme are presented in **Figure 5** and **Figure S4** of Supporting Information. The positive charge in Au_4^+ is roughly equally distributed over the Au atoms. Upon doping, Pd draws electron density from the Au atoms, which gives Pd a formal negative charge in $PdAu_3^+$. In Au_5^+, however, due to its high symmetry, the central Au atom has zero net positive charge and in $PdAu_4^+$ the central Au atom draws most of the charge, reducing the charge available to the Pd atom, and hence it's influence on the cluster's electronic properties. In fact, even though $PdAu_4^+$ has a 3D structure, the average bond length between Au atoms in the cluster is not notably affected by the Pd dopant, being 2.63 Å for both $PdAu_4^+$ and Au_5^+. This situation is different for Au_4^+ and $PdAu_3^+$, with average Au–Au distances of 2.66 Å and

2.72 Å, respectively. An overview of the calculated average bond distances is available in **Table S1** of the Supporting Information.

4.2. Orbital analysis of optical transitions

4.2.1 Au_4^+ and $PdAu_3^+$ clusters

The suppression of the optical response on Pd doping is investigated by calculation of the states that make up the relevant region of the band structure. In **Figure 6**, a representative electronic correlation diagram is shown for Au_4^+, $PdAu_3^+$, and Pd_4^+. For the case of Pd_4^+, the lowest energy structure is calculated as a Jahn-Teller distorted tetrahedron, with bonds of 2.72 Å in the basal plane, and a compressed z direction with bonds of 2.64 Å to the top atom.

The Au_4^+ cluster shows a significant degree of s-d mixing, which is primarily manifested at the top (0 eV) and bottom (-4.8 eV) of the d band, as well as in intermediate peaks throughout the band. The bands are molecular, due to the small size of the cluster, and thus molecular charge-transfer transitions, which result from the differences in electronic structure between non-equivalent atoms, may be resolved. One example is the s-d → s-d transition from a hinge atom (0 eV) to the wingtip atom at +0.1 eV. For the Pd_4^+ cluster, the s-d mixing is diminished. The HOMO state is of 100% d character, and the first filled s state is at -1.5 eV. Therefore, interband s → d and d → s transitions, as well as intraband s → s transitions are likely to be suppressed in Pd clusters. The doped $PdAu_3^+$ cluster represents an intermediate case, in which the width of the d band is between that of Au_4^+ and Pd_4^+, and some s-d mixing is present due to the Au atoms. The first filled s state is at -0.9 eV, which lies between the values for the two monoelemental clusters, and represents a significant increase in energy required for optical transitions from s states as compared to Au_4^+. The energy gap to s-like conduction band states is similarly increased, from 1.1 eV in Au_4^+ to 1.8 eV in $PdAu_3^+$. This overall depletion of s density near the Fermi energy is likely a major cause for the suppression of the optical absorption bands.

4.2.2 Au_4^+Ar and $PdAu_3^+$Ar clusters

Upon Pd doping, the electronic character of the calculated transitions of $PdAu_3^+$Ar is changed significantly with respect to the Au_4^+Ar cluster. The introduction of Pd allows for intraband sp-sp transitions, which occur between elements. Peak A of Figure 3c corresponds to an Au to Pd transition, with elemental contributions of 95/5/0 in the initial state, and 20/79/1 in the final state (Au/Pd/Ar percentages). Peak B, in contrast, is a Pd to Au transition, with elemental contributions of 34/65/1 and 85/15/0 in the initial and final states, respectively.

4.2.3 Au_5^+Ar and $PdAu_4^+$Ar clusters

For the Pd-doped cluster $PdAu_4Ar^+$, peak A at 3.57 eV (Figure 4b) consists of Au(sd) to Pd(p) interatomic charge transfer character. The bands of higher energy transitions in the range 3.8-4.3 eV also have primarily Au-Pd character. Charge transfer transitions therefore occur in the same interelemental manner, and involve the same orbitals as for the 4-atom metal clusters. However, it should be noted that for the global minimum cluster structure found for $PdAu_4Ar^+$, the total static charge transfer from Au to Pd, from Löwdin analysis, is found to be less extensive than for the smaller clusters. The MO pair which contributes most to the (lowest energy) transition at 3.85 eV in Au_5^+Ar has a weight of 93% Au and 7% Ar in the initial state, and 73% Au, 27% Ar in the final state. The greatest atomic orbital weights for this peak are, however, located on Au atoms, with Au d_{xz}/d_{yz} and Au sp the largest contributors in the initial and final states, respectively. For the higher energy peaks at 4.08 and 4.32 eV, the MO pairs involve Au d orbitals as the major component of the initial state, and Au sp orbitals in the final state. The excitation with large oscillator strength at 4.60 eV has a slightly different character, consisting of Au sp (85% on Au) to Au s (95% on Au) transition.

4.4. Conclusion

In this article we have presented a combined photodissociation spectroscopy and time-dependent density functional theory study of the effect of Pd doping on the structures and optical absorption of the small cationic gold clusters Au_4^+, Au_4^+Ar and Au_5^+Ar.

Whereas the structures of pure cationic gold clusters are planar, the Pd-doped clusters were found to be 3-dimensional. An analysis of electron density transfers showed the very different influence of the Pd dopant in the tetrameric and pentameric clusters. While Pd draws so much charge from the Au atoms that it becomes negatively charged in $PdAu_3^+$, the Pd atom in $PdAu_4^+$ has a positive charge that is higher than the charge of the highly coordinated central Au atom.

Photoabsorption spectra were recorded using photon induced fragmentation of the clusters, in the broad energy range of 2.0 to 4.7 eV, allowing the observation of previously unreported absorption bands for Au_4^+ and Au_4^+Ar clusters. The inclusion of a single Pd atom changed the optical absorption spectra of Au_4^+ and Au_4^+Ar drastically, quenching most absorption features, in contrast to the less pronounced effect for the pentameric system.

The observed quenching effect in $PdAu_3^+$ was attributed to structural changes induced by the dopant atom in addition to alterations in the cluster‘s electronic structure. For pure Au_4^+, a significant s-d mixing is observed, which is diminished upon Pd doping. These effects, however, are size dependent. The structure of Au_5^+ is less affected by the addition of Pd. The smaller charge transfer induced by the dopant in this cluster is reflected in a small effect on the optical absorption.

Supporting Information

Supporting Information is available online from the Wiley Online Library or from the author.

Acknowledgements

This work is supported by the Research Foundation-Flanders (FWO), by the KU Leuven Research Council (BOF program and grant number GOA/14/007), and by the COST Action MP0903 “Nanoalloy”. P. Ferrari acknowledges CONICyT for a Becas Chile scholarship. The calculations reported were performed using the University of Birmingham BlueBEAR HPC facility.[61]

Received: ((will be filled in by the editorial staff))
Revised: ((will be filled in by the editorial staff))
Published online: ((will be filled in by the editorial staff))

[1] H. M. Chen, C. K. Chen, C. Chen, L. Cheng, P. C. Wu, B. H. Cheng, Y. Z. Ho, M. L. Tseng, Y. Hsu, T. Chan, J. Lee, R. Liu and D. P. Tsai, *ACS nano* **2012**, *6*, 7362.

[2] W. H. Hung, M. Aykol, D. Valley, W. Hou and S. B. Cronin, *Nano Lett.* **2010**, *10*, 1314.

[3] D. Panayotov, S. Burrows, J. T. YatesJr and J. R. Morris, *J. Phys. Chem. C* **2011**, *115*, 22400.

[4] Y. Chen, H. Choi and P. V. Kamat, *J. Am. Chem. Soc.* **2013**, *135*, 8822.

[5] A. P. Woodham and A. Fielicke, *Gold Clusters, Colloids and Nanoparticles I*, Vol. 161 (Eds: D. Michael, P. Mingos), Springer International Publishing, Switzerland **2014**, pp 243-278.

[6] W. A. de Heer, Rev. *Mod. Phys.* **1993**, *65*, 611.

[7] S. M. Lang and T. M. Bernhardt, *Phys. Chem. Chem. Phys.* **2012**, *14*, 9255.

[8] S. Gilb, P. Weis, F. Furche, R. Ahlrichs and M. M. Kappes, *J. Chem. Phys.* **2002**, *116*, 4094.

[9] P. Gruene, D. M. Rayner, B. Redlich, A. F. G. van der Meer, J. T. Lyon, G. Meijer and A. Fielicke, *Science* **2008**, *321*, 674.

[10] M. P. Johansson, A. Lechtken, D. Schooss, M. M. Kappes and F. Furche, *Phys. Rev. A* **2008**, *77*, 053202.

[11] H. Häkkinen, B. Yoon, U. Landman, X. Li, H. J. Zhai and L. S. Wang, *J. Phys. Chem. A* **2003**, *107*, 6123.

[12] A. V. Walker, *J. Chem. Phys.* **2005**, *122*, 094310.

[13] S. Lecoultre, A. Rydlo, C. Félix, J. Buttet, S. Gilb and W. Harbich, *J. Chem. Phys.* **2011**, *134*, 074303.

[14] M. Harb, F. Rabilloud, D. Simon, A. Rydlo, S. Lecoultre, F. Conus, V. Rodrigues and C. Félix, *J. Chem. Phys.* **2008**, *129*, 194108.

[15] S. Lecoultre, A. Rydlo, J. Buttet, C. Félix, S. Gilb and W. Harbich, *J. Chem. Phys.* **2011**, *134*, 184504.

[16] S. Lecoultre, A. Rydlo, C. Félix, J. Buttet, S. Gilb and W. Harbich, *J. Chem. Phys.* **2011**, *134*, 074302.

[17] A. Terasaki, T. Majima, C. Kasai and T. Kondow, *Eur. Phys. J. D* **2009**, *52*, 43.

[18] F. Conus, V. Rodrigues, S. Lecoultre, A. Rydlo and C. Félix, *J. Chem. Phys.* **2006**, *125*, 024511.

[19] A. Schweizer, J. M. Weber, S. Gilb, H. Schneider, D. Schooss and M. M. Kappes, *J. Chem. Phys.* **2003**, *119*, 3699.

[20] A. N. Gloess, H. Schneider, J. M. Weber and M. M. Kappes, *J. Chem. Phys.* **2008**, *128*, 114312.

[21] G. Stefan, K. Jacobsen, D. Schooss, F. Furche, R. Ahlrichs and M. M. Kappes, *J. Chem. Phys.* **2004**, *121*, 4619.

[22] A. Shayeghi, R. L. Johnston and R. Schafer, *Phys. Chem. Chem. Phys.* **2013**, *15*, 19715.

[23] A. Shayeghi, D. A. Gotz, R. L. Johnston and R. Schafer, *Eur. Phys. J. D* **2015**, *69*, 152.

[24] M. B. Knickelbein, *J. Chem. Phys.* **199**4, *100*, 4729.

[25] P. Pyykko, *Chem. Rev.* **1988**, *88*, 563.

[26] E. Janssens and P. Lievens, *Adv. Nat. Sci.: Nanosci. Nanotechnol.* **2011**, *2*, 023001.

[27] N. Veldeman, E. Janssens, K. Hansen, J. D. Haeck, R. E. Silverans and P. Lievens, *Faraday Discuss.* **2008**, *138*, 147.

[28] H. T. Le, S. M. Lang, J. D. Haeck, P. Lievens and E. Janssens, *Phys. Chem. Chem. Phys.* **2012**, *14*, 9350.

[29] D. W. Yuan, Y. Wang and Z. Zeng, *J. Chem, Phys.* **2005**, *122*, 114310.

[30] G. A. Bishea and M. D. Morse, *J. Chem. Phys* **1991**, *95*, 5646.

[31] G. A. Bishea, J. C. Pinegar and M. D. Morse, *J. Chem. Phys.* **1991**, *95*, 5630.

[32] S. M. Lang, P. Claes, N. T. Cuong, M. T. Nguyen, P. Lievens and E. Janssens, *J. Chem. Phys.* **2011**, *135*, 224305.

[33] A. Shayeghi, C. J. Heard, R. L. Johnston and R. Schafer, *J. Chem. Phys.* **2014**, *140*, 054312.

[34] K. Koyasu, M. Mitsui, A. Nakajima and K. Kaya, *Chem. Phys. Lett.* **2002**, *358*, 224.

[35] S. M. Lang, A. Frank, I. Fleischer and T. M. Bernhardt, *Eur. Phys. J. D* **2013**, *67*, 1.

[36] Z. J. Wu, S. H. Zhou, J. S. Shi and S. Y. Zhang, *Chem. Phys. Lett.* **2003**, *368*, 153.

[37] G. Zanti and D. Peeters, *J. Phys. Chem. A* **2010**, *114*, 10345.

[38] B. R. Sahu, G. Maofa and L. Kleinman, *Phys. Rev. B* **2003**, *67*, 115420.

[39] Z. Wang, J. Jia and H. Wu, *Mater. Chem. Phys.* **2015**, *160*, 105.

[40] T. Balcha, J. R. Strobl, C. Fowler, P. Dash, and R. W. J. Scott, *ACS Catal.* **2011**, *1*, 425.

[41] F. Liu, D. Wechsler, and P. Zhang, *Chem. Phys. Lett.* **2008**, *461*, 254.

[42] V. Kaydashev, E. Janssens and P. Lievens, *J. Chem. Phys.* **2015**, *142*, 034310.

[43] W. Bouwen, P. V. F. Thoen, S. Bouckaert, F. Despa, H. Weidele, R. E. Silverans and P. Lievens, *Rev. Sci. Instrum.* **2000**, *71*, 54.

[44] S. M. Lang, P. Claes, S. Neukermans and E. Janssens, *J. Am. Soc. Mass Spectrom.* **2011**, *22*, 1508.

[45] R. L. Johnston, *Dalton Trans.* **2003**, *22*, 4193.

[46] P. Giannozzi et al., *J. Phys.: Condens. Matter* **2009**, *21*, 395502.

[47] J. P. Perdew, K. Burke and M. Ernzerhof, *Phys. Rev. Lett.* **1996**, *77*, 3865.

[48] A. M. Rappe, K. M. Rabe, E. Kaxiras and J. D. Joannopoulos, *Phys. Rev. B* **1990**, *41*, 1227.

[49] M. Valiev, E. Bylaska, N. Govind, K. Kowalski, T. Straatsma, H. Van Dam, D. Wang, J. Nieplocha, E. Apra, T. Windus and W. de Jong, *Comput. Phys. Commun.* **2010**, *181*, 1477.

[50] F. Weigend and R. Ahlrichs, *Phys. Chem. Chem. Phys.* **2005**, *7*, 3297.

[51] O. A. Vydrov and G. E. Scuseria, *J. Chem. Phys.* **2006**, *125*, 234109.

[52] M. A. Rohrdanz, K. M. Martins and J. M. Herbert, *J. Chem. Phys.* **2009**, *130*, 054112.

[53] L. Skripnikov, Chemissian, *A Computer Program to Analyse and Visualise Quantum-Chemical Calculations*, **2012**.

[54] J. U. Andersen, E. Bonderup, K. Hansen, P. Hvelplund, B. Liu, U. V. Pedersen and S. Tomita, *Eur. Phys. J. D* **2003**, *24*, 191.

[55] A. Shayeghi, R.L. Johnston, D.M. Rayner, R. Schäfer and A. Fielicke, *Angew. Chem. Int. Ed.* **2015**, *54*, 10675.

[56] B. Kalita and R. C. Deka, *J. Chem. Phys.* **2007**, *127*, 244306.

[57] S. Heiles, A. J. Logsdail, R. Schäfer and R. L. Johnston, *Nanoscale* **2012**, *4*, 1109.

[58] S. Zhao, X. Tian, J. Liu, Y. Ren and J. Wang, *Comp. Theor. Chem.* **2015**, *1055*, 1.

[59] S. Peng, L. Gan, R. Tian and Y. Zhao, *Comp. Theor. Chem.* **2011**, *977*, 62.

[60] S. Öğüt, J. C. Idrobo, J. Jellinek, J. Wang, *J. Cluster Sci.* **2006**, *17*, 609.

[61] University of Birmingham, Birmingham Environment for Academic Research, http://www.bear.bham.ac.uk/bluebear (accessed 01, 2016).

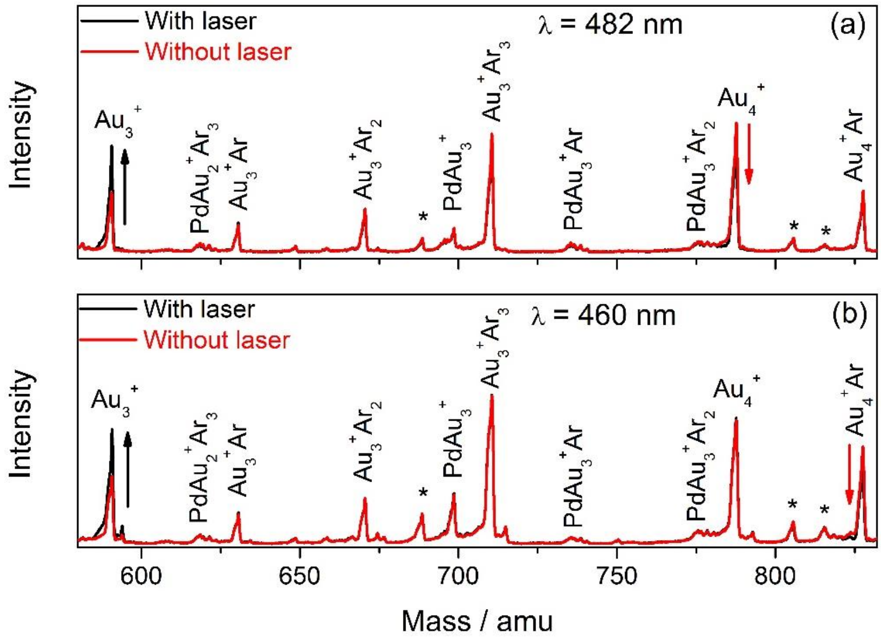

Figure 1. Mass spectra with (black) and without (red) laser excitation at (a) 480 nm and (b) 460 nm. The decrease in signal for Au_4^+ at 482 nm and for Au_4^+Ar at 460 nm (indicated by an arrow) implies laser induced fragmentation of these clusters. In contrast, the increase in Au_3^+ signal shows that this cluster is the fragmentation channel of Au_4^+ (at 482 nm). The similar increase of Au_3^+ at λ=460 nm proves that Au_3^+ is also a product ion of the fragmentation of Au_4^+Ar. The * correspond to oxygen contaminated clusters.

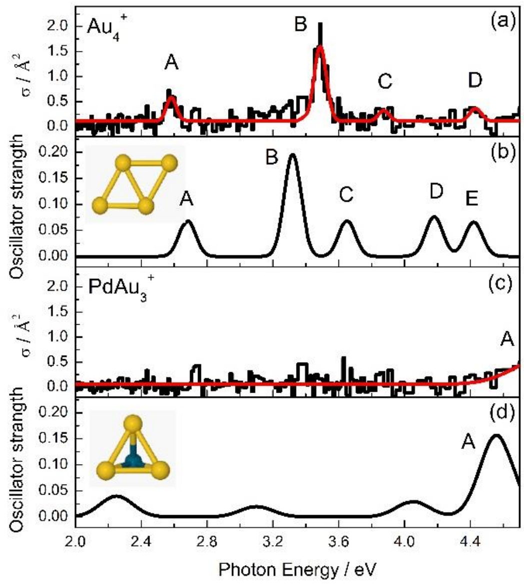

Figure 2. Comparison of experimental photodissociation ((a) and (c)) and calculated electronic excitation ((b) and (d)) spectra of the lowest energy isomers for Au_4^+ and $PdAu_3^+$. Black step lines represent the experimental data while red solid lines are multi-Gaussian fits. Absorption cross sections are obtained by Equation 1 from measured photodepletions. The corresponding lowest energy isomers are displayed as insets in the figure with Au atoms shown in yellow and Pd in blue.

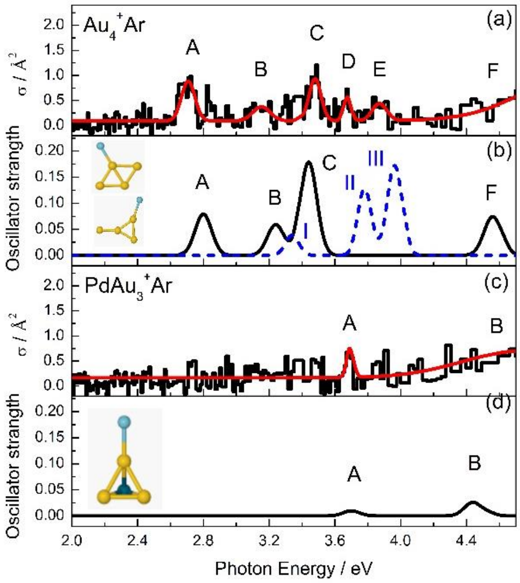

Figure 3. Comparison of experimental photodissociation ((a) and (c)) and calculated electronic excitation ((b) and (d)) spectra of the lowest energy isomers for Au_4^+Ar and $PdAu_3^+Ar$. Black step lines represent the experimental data while red solid lines are multi-Gaussian fits. Absorption cross sections are obtained by Equation 1 from measured photodepletions. The corresponding lowest energy isomers are displayed as insets in the figure with Au atoms shown in yellow, Pd in blue and Ar in sky-blue. In (b) the Y-shaped isomer of Au_4^+Ar, 0.11 eV higher in energy than the global minimum, is shown by dashed blue line.

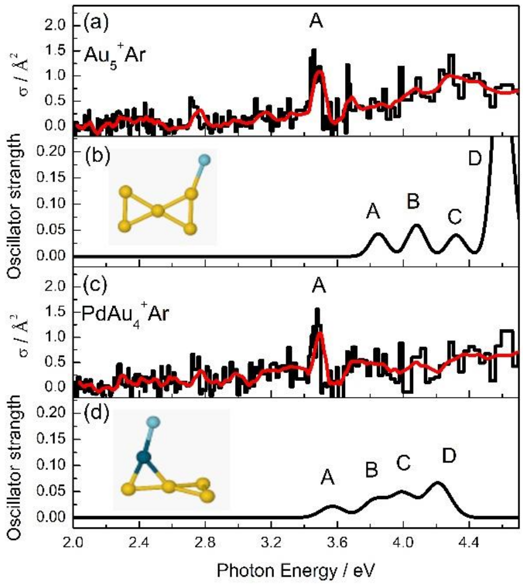

Figure 4. Comparison between experimental photodissociation and calculated electronic excitation spectra of the lowest energy isomer for Au_5^+Ar and $PdAu_4^+Ar$. In (a) and (c) experimental spectra are presented for Au_5^+Ar and $PdAu_4^+Ar$, respectively. Black step lines

represent the experimental data while solid lines an averaged curve of 3-adjacent points. Absorption cross sections are obtained by Equation 1 from the measured photodepletions. In addition, (b) and (d) show calculated spectra for Au_5^+Ar and $PdAu_4^+Ar$, respectively. The corresponding lowest energy isomers are displayed as insets in the figure with Au atoms shown in yellow, Pd in blue and Ar in sky-blue.

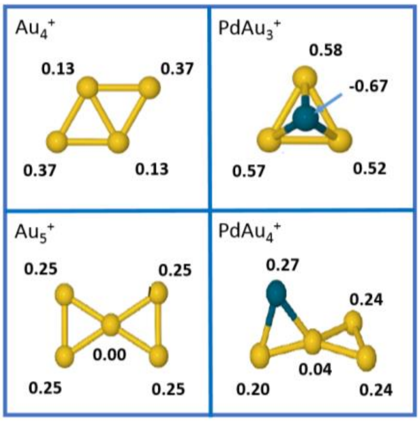

Figure 5. Calculated atomic charges of the lowest energy structures of Au_n^+ and $PdAu_{n-1}^+$ (n = 4, 5) using the Löwdin scheme. Au atoms are shown in yellow and Pd in blue.

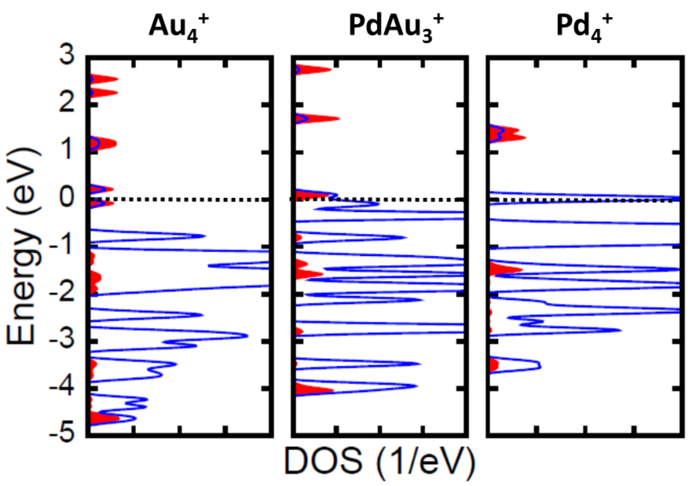

Figure 6. Projected density of states for Au_4^+, $PdAu_3^+$ and Pd_4^+, calculated at the PBE level of theory. Electron density is projected onto s (filled red lines) and d (blue lines) atomic orbitals, and presented relative to the Fermi energy (dashed black line).

Table 1. Most favorable fragmentation channels and their corresponding dissociation energies obtained by DFT calculations.

Mother species	Fragments	Dissociation energy [eV]
Au_4^+	Au_3^+ + Au	1.33
$PdAu_3^+$	$PdAu_2^+$ + Au	2.25
Au_4^+Ar	Au_4^+ + Ar	0.21
Au_4^+Ar	Au_3^+ + Au + Ar	1.54
$PdAu_3^+Ar$	$PdAu_3^+$ + Ar	0.23
$PdAu_3^+Ar$	$PdAu_2^+$ + Pd + Ar	2.58
Au_5^+	Au_3^+ + Au_2	2.17
$PdAu_4^+$	$PdAu_3^+$ + Au	1.64
Au_5^+Ar	Au_5^+ + Ar	0.21
$PdAu_4^+Ar$	$PdAu_3^+$ + Ar	0.23

Table 2. Peak positions and oscillator strengths of the absorption bands for the studied clusters. Peaks are labelled according to Figure 1, 2 and 3. Experimental oscillator strengths are calculated by $f = 0.91103 \int d(E)dE$ and the Gaussian fits of the experimental data.[19,21]

	Peak	Position (eV)		Oscillator strength	
		Exp.	Theory	Exp.	Theory
Au_4^+	A	2.58 ± 0.01	2.68	0.033 ± 0.006	0.070
	B	3.49 ± 0.01	3.32	0.125 ± 0.007	0.200
	C	3.87 ± 0.02	3.65	0.016 ± 0.009	0.070
	D	4.43 ± 0.02	4.18	0.011 ± 0.009	0.080
	E		4.42		0.080
$PdAu_3^+$	A	> 4.70	4.56	> 0.080	0.170
Au_4^+Ar	A	2.71 ± 0.01	2.80	0.074 ± 0.009	0.080
	B	3.15 ± 0.02	3.24	0.034 ± 0.012	0.060
	C	3.48 ± 0.01	3.44	0.070 ± 0.009	0.180
	D	3.67 ± 0.01		0.023 ± 0.009	
	E	3.87 ± 0.02		0.035 ± 0.013	
	F	> 4.70	4.56	> 0.070	0.080
$PdAu_3^+Ar$	A	3.69 ± 0.02	3.70	0.028 ± 0.005	0.009
	B	> 4.70	4.44	> 0.100	0.026
Au_5^+Ar	A	3.46 ± 0.01	3.85	0.089 ± 0.010	0.045
	B		4.08		0.063
	C		4.32		0.043

	D		4.60		0.467
$PdAu_4^+Ar$	A	3.48 ± 0.03	3.57	0.077 ± 0.009	0.022
	B		3.83		0.035
	C		4.00		0.048
	D		4.24		0.020

The effect of a single Pd dopant atom in the optical absorption of the small gas phase Au_4^+ and Au_5^+ clusters is studied by a combination of photodissociation spectroscopy and density functional theory calculation. A quenching of most absorption bands is observed and attributed to charge transfers and structural changes induced by the Pd dopant atom.

Optical absorption

V. Kaydashev, P. Ferrari, C. Heard, E. Janssens*, R. L. Johnston, and P. Lievens

Optical absorption of small palladium doped gold clusters

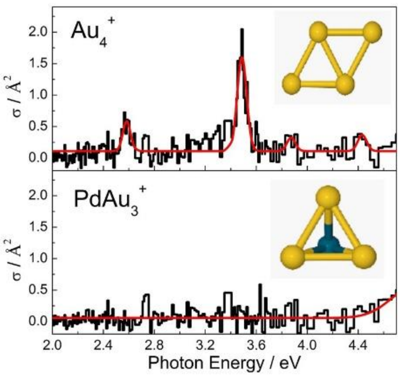

Figure 1

Click here to access/download
Production Data
Fig1.tif

Figure 2

Click here to access/download
Production Data
Fig2.tif

Figure 3

Click here to access/download
Production Data
Fig3.tif

Figure 4

Click here to access/download
Production Data
Fig4.tif

Figure 5

Click here to access/download
Production Data
Fig5.tif

Figure 6

Click here to access/download
Production Data
Fig6.tif

ToC

Click here to access/download

Production Data

ToC.tif